Vacuum 215 (2023) 112338

Contents lists available at ScienceDirect

Vacuum

journal homepage: www.elsevier.com/locate/vacuum

Microstructural evolution of TiC nano powders under fast neutron irradiation: A multi-technique analysis

E. Popov [a,b,c], L. Slavov [d], E. Demir [e,f], B.A. Abdurakhimov [c,g], A.S. Doroshkevich [c], O.A. Aliyev [h], S.H. Jabarov [i], A.H. Valizade [i], B. Mauyey [c,j], P. Horodek [k], K. Siemek [k], O. Samedov [i], M. N. Mirzayev [i,l,m,*]

[a] Institute of Solid-State Physics, Bulgarian Academy of Sciences, Sofia, 1784, Bulgaria
[b] Institute for Nuclear Research and Nuclear Energy, Bulgarian Academy of Sciences, Sofia, 1784, Bulgaria
[c] International Intergovernmental Organization Joint Institute for Nuclear Research, Dubna, 141980, Russia
[d] Institute of Electronics, Bulgarian Academy of Sciences, Sofia, 1784, Bulgaria
[e] Yeditepe University, Physics Department, Istanbul, 34755, Turkey
[f] Department of Nuclear Engineering, North Carolina State University, Raleigh, NC, 27607, USA
[g] Institute of Nuclear Physics, Academy of Sciences of Uzbekistan, Tashkent, 100214, Uzbekistan
[h] Institute of Physics Ministry of Science and Education Republic of Azerbaijan Baku, AZ-1143, Azerbaijan
[i] Institute of Radiation Problems, Ministry of Science and Education Republic of Azerbaijan, Baku, AZ1143, Azerbaijan
[j] L.N. Gumilyov Eurasian National University, Astana, 010008, Kazakhstan
[k] Institute of Nuclear Physics Polish Academy of Sciences, PL-31342, Krakow, Poland
[l] Western Caspian University, Baku, AZ1001, Azerbaijan
[m] Scientific-Research Institute Geotecnological Problems of Oil, Gas and Chemistry, Azerbaijan State Oil and Industry University, Baku, AZ-1010, Azerbaijan

ARTICLE INFO

Handling Editor: Prof. L.G. Hultman

Keywords:
Nano crystal titanium carbide
Neutron irradiation
Raman
FTIR
TEM
SAED

ABSTRACT

In this work, titanium carbide nano powders were irradiated at normal conditions of 293.15 K and 1 atm with fluencies of 4.0×10^{12} n/cm^2, 8.0×10^{12} n/cm^2, 1.3×10^{13} n/cm^2, 4.0×10^{14} n/cm^2, and 10^{15} n/cm^2 (neutron energy 1 MeV). The microstructure of the titanium carbide nano powders after irradiation was examined using X-ray diffraction, Raman spectroscopy, and FTIR spectroscopic analysis methods. The X-ray diffraction analysis revealed that no significant phase transition or amorphization occurred in the TiC nano powders exposed to fast neutrons. More sensitive results obtained from the FTIR analysis showed that the water molecules absorbed on the material surface were disintegrated under the influence of fast neutrons. Exceptional structural stability to neutron irradiation of titanium carbide without amorphization was also observed by morphological analysis via transmission electron microscopy (TEM) and selected area electron diffraction (SEAD).

1. Introduction

Titanium carbide (TiC) is a transition metal carbide with a rock-salt crystal structure, which has gained significant attention as a material for use in extreme environments due to its high melting temperature, hardness, and thermal/electrical conductivity [1–6]. TiC, as an ultra-high-temperature ceramic (UHTC), is widely utilized for fabricating cutting tools, heat-resistant hard alloys, abrasive, and anti-wear materials [3,7,8]. Moreover, TiC exhibits high mechanical resistance, good fission product confinement, and small neutron capture cross-sections [6,9–11], making it a promising candidate for use as a matrix material for inert matrix fuel (IMF) in gas-cooled fast reactors (GFR) and as a structural material in nuclear reactor technology [4–6,11–15]. However, any material utilized in nuclear technologies must be able to withstand the harsh nuclear reactor environment, which includes constant bombardment by hydrogen isotopes, helium, and incident neutrons [1,3,6,11,16], to meet the high expectations. Although TiC appears to satisfy the necessary physical and chemical criteria outlined by Agarwal et al. [1], its suitability as a material must be evaluated based on its irradiation resistance, which requires multiple real-time experiments. Surprisingly few experiments have been conducted to test the irradiation resistance of TiC, despite suggestions dating back to the mid-1960s that TiC holds significant potential as a structural element in nuclear technologies. Koval'chenko and Ogorodnikov [17]

* Corresponding author. Institute of Radiation Problems, Azerbaijan National Academy of Sciences, Baku, AZ1143, Azerbaijan.
E-mail address: matlabmirzayev@gmail.com (M.N. Mirzayev).

https://doi.org/10.1016/j.vacuum.2023.112338
Received 28 April 2023; Received in revised form 8 June 2023; Accepted 17 June 2023
Available online 19 June 2023

suggested in 1966 that studying the structural defects resulting from neutron irradiation experiments is the best way to determine whether TiC can be utilized in a nuclear reactor or as a component of the first wall. Only one article has been published on this subject in the last 30 years [1], and the total number of available studies does not exceed ten. Table 1 summarizes the specific experimental irradiation conditions utilized by various groups and one critical characteristic of TiC, its stoichiometry (when available).

Agarwal et al. [1] have emphasized that the development of point defects in the crystal structure of TiC and their subsequent evolution into two- and three-dimensional defects are directly linked to temperature and radiation dose (or fluence). When discussing and comparing changes occurring in TiC structure due to neutron irradiation, it is important to consider the energy of neutrons used in the experiment, as shown in Table 1. Despite the limited number of investigations, the experimental conditions cover almost all the pre-conditioning necessary to evaluate the neutron irradiation effects on the material. The investigations used fast neutrons (>0.1 MeV) [1,17–20], fusion neutrons (~14 MeV) [21–23], and even thermal neutrons (0.025 eV) [24] for irradiation of TiC (Table 1). It should be noted that in studies conducted before 1980, the reported temperatures of the samples studied were mostly a consequence of the introduced irradiation at room temperature. During the next decade of neutron irradiation experiments, low-temperature investigations aimed at fundamental physical insight into the changes in the crystal lattice, as well as those carried out by irradiating the samples with 14 MeV neutrons to simulate damage in a real nuclear reactor environment, were focused upon [20–23]. All investigations included fluencies above 10^{16} n/cm^2 (Table 1). As a result of neutron irradiations, ambiguous changes have been reported, including changes in the parameters of the crystal lattice with increasing dose and some physical characteristics (e.g., electrical resistance) of TiC. While Koval'chenko and Ogorodnikov [17] observed a decrease in mean grain size upon irradiation, a subsequent study [19], by largely the same scientific team, concluded that neutron irradiation leads to an increase in the lattice parameters in TiC under identical conditions in both experiments (Table 1). G. W. Keilholtz et al. [18] and M.S. Kova'lchenko et al. [24] both report an initial increase in the TiC crystal volume with subsequent contraction or retention of the new values reached upon irradiation. Other important findings include a linear increase in the electrical resistivity [17,20,24] and the micro hardness [17] with increasing irradiation dose. On the other hand, H. Matsui et al. [21] describe their observations on electrical resistivity as "almost" linear with increasing fluence, with some initial decrease in the values for the resistivity for their $TiC_{0.72}$ specimen. In their further investigations, Matsui et al. [22,23] concluded that non-stoichiometry of the compound is a major factor in considering the induced damage with irradiation. The higher carbon content means more induced damage and thus an increase in the electrical resistivity [21–23]. The differences in the observed changes of the crystal lattice parameters could also be explained by differences in the stoichiometry of the studied samples in the different experiments. In all cases, the neutron irradiation induced point defects and their evolution are described as the major factors driving the damage levels. Such evolution could manifest as an increase in the mobility of vacancies or interstitials leading to their accumulation and agglomeration or clustering and swelling [1,18,19]. At the same time, annihilation by recombination of point defects with structural carbon vacancies [23] could occur in parallel as a kind of opposite or "healing" process.

This complex phenomenon requires extensive scientific research on the defects induced by irradiation, especially considering the numerous advanced methods available for characterization and analysis. Furthermore, given the rapid development of nuclear and nanotechnologies, previous qualitative research conducted before 1991 [17–24] has limitations in terms of application due to the strong possibility that commercially available TiC products today may differ significantly from those studied more than three decades ago, with regards to preparation methods and resulting products. To address this gap, recent research by S. Agarwal et al. [1] investigated the microstructural degradation process in TiC using TEM and HRTEM analysis, which was not done in previous neutron irradiation studies. The authors observed two types of

Table 1
Overview of published neutron real-time experiments conducted through the last 60 years.

Year of research publication	Reference	Energy of neutrons used for irradiation, [MeV]	Fluence, [n/cm^2]	Temperature during irradiation[a]	TiC stoichiometry (if available)
1966	M.S. Koval'chenko and V. V. Ogorodnikov [17]	>0.1	10^{16} 10^{20}	<100 °C	Not specified
1968	G. W. Keilholtz et al. [18]	>1	0.8×10^{21} to 5.4×10^{21}	300–700 °C	Not specified[b]
1972	M.S. Kova'lchenko et al. [24]	Thermal neutrons (0.025 eV), Th.n/f.n = 8/1	1.0×10^{19} 3.7×10^{19} 7.5×10^{19} 1.5×10^{20}	50 °C	$TiC_{0.94}$
1974	M.S. Koval'chenko et al. [19]	>0.1	10^{16} 10^{18} 10^{20}	0–1200 °C During annealing	Not specified
1981	J. Morilo et al. [20]	>1	1.3×10^{18} 1.8×10^{18}	21 K; followed by annealing up to 400 K	$TiC_{0.97}$
1985	H. Matsui et al. [21]	14	0.97×10^{17} 1.92×10^{17}	4–5.5 K (LHeT); followed by annealing up to 340 K	$TiC_{0.56}$ $TiC_{0.66}$ $TiC_{0.72}$
1988	H. Matsui and M. Iseki [22]	14	6.1×10^{16} 3.3×10^{17} 1.0×10^{18} 2.0×10^{18} 3.5×10^{18}	RT	$TiC_{0.66}$ $TiC_{0.72}$ $TiC_{1.00}$
1991	H. Matsui et al. [23]	14	In-situ measurements up to 1.92×10^{17} at intervals of roughly 1.5×10^{15}	LHeT (for nonst.) RT (for st.) 723 K	$TiC_{0.56}$ $TiC_{0.66}$ $TiC_{0.72}$ $TiC_{1.00}$
2020	S. Agarwal et al. [1]	>0.1	1.97×10^{21} 2.16×10^{21} 2.24×10^{21}	220 °C 620 °C 1115 °C	$TiC_{0.80}$[c]

[a] Units given as in the original article;
[b] Data is available on the "total" and "free" carbon in the specimens under investigation in wt %;
[c] The value is based on comparing Raman spectra.

dislocation loops formed during irradiation, depending on the temperature, and no amorphization of the specimen at any of the conditions used. It is worth noting that in addition to neutron irradiation, the material is also subjected to bombardment with hydrogen and helium ions, as they are participants in the fusion reaction. In our study, we used a combination of various characterization techniques, including X-ray diffraction (XRD), Raman spectroscopy, Fourier-transform infrared spectroscopy (FTIR), and transmission electron microscopy (TEM), to comprehensively evaluate the microstructure of commercially available nanosized TiC before and after fast neutron irradiation (>0.1 MeV) at room temperature and fluence values not previously reported, ranging from 4.0×10^{12} n/cm^2 to 10^{15} n/cm^2. Special attention was given to the degree of amorphization resulting from irradiation and the extent of surface oxidation of the material, which have not been addressed in previous research.

Positron annihilation, due to its non-destructive approach and high sensitivity to structural defects, is an essential method in materials science and solid-state research [25]. The trapping model is a theoretical approach used to explain the processes involved in positron research. When positrons enter a solid, they are trapped by the defects in the crystal lattice [26], where the electron density is lower than the average volume. The lifetime values of a positron trapped in vacancy clusters differ from those of a positron trapped in nano-voids that contain helium or hydrogen. However, our powdered samples posed a significant challenge in conducting a real experiment. Therefore, our study focused on analyzing the defects' evolution through model calculations. In this manner, it was examined the penetration of hydrogen and helium into the material by using model calculations, while the consequences of neutron irradiation were studied through a real experiment.

2. Materials and methods

The nano titanium carbide samples were thermal annealing at 1200 °C for 2 h in a Linn™ HT-1800 high-temperature controlled atmosphere furnace with a heating and cooling rate of 5 °C/min under vacuum (10^{-6} Tr), followed by inert Ar gas conditions. The microstructure of the samples was analyzed by utilizing transmission electron microscopy (TEM) and scanning electron microscopy (SEM) with JEM 200 A and JSM640LV (JEOL, Japan) instruments, respectively. The investigation focused on commercially available powdered, nan sized titanium carbide (Sigma-Aldrich, Germany) with a purity of 99.999%, a bulk density of 0.069 g/cm^3, a specific surface area of 70–90 m^2/g, and a particle size larger than 100 nm. Aluminum foil was used to envelop the samples, which were then irradiated at different doses. Neutron irradiation was performed at normal conditions (293.15 K, 1 atm) at fluencies of 4.0×10^{12} n/cm^2, 1.3×10^{13} n/cm^2, 4.0×10^{14} n/cm^2, and 10^{15} n/cm^2 (neutron energy 1 MeV) at the IBR-2 high-flux pulsed reactor at Frank Laboratory of Neutron Physics (JINR, Dubna, Russia) [27–30]. The γ dose rate was approximately 500 Gy/h, which accounted for about 85% of the total dose [31,32]. Structural characteristics of the samples were measured using the XRD EMPYREANPAN analytical diffractometer with a CuKα source (λ = 1.5406 Å). The tube of the diffractometer with a copper anode was set to U = 40 kV voltage and generated a current of I = 40 mA [33,34]. The Rietveld analysis of X-ray diffraction patterns was carried out using the FullProf software package. Raman spectroscopy experiments were performed at room temperature using an INTEGRA Spectra LS PNL instrument [35]. The Raman spectrometer SOLAR TII was excited with a 633 nm Helium–Neon laser with up to 35 mW output power, and the wavelength resolution was 0.03 nm. Spectra were collected from at least 7 different points for each specimen for optimal statistics. FTIR experiments were performed using the Thermo Scientific™ Smart™ iTX ATR Accessory instrument [30].

The positron lifetime was determined using the MIKA (Multi-grid Instead of the K-spAce) package [36], which utilizes a two-component expansion of density functional theory (TCDFT) and a local density approximation (LDA) method. The calculation was carried out with fixed TiC unit cell parameters of a, b, c = 4.3305 Å and α, β, γ = 90°. The TiC material has a face-centered cubic (FCC) crystal structure with Fm/3 m (225) group symmetry [37]. Specifically, attention was given to the portion of the general functional that governs the exchange-correlation interaction [38–40]:

$$E_{xc}[n(r)] = \int n(r)\varepsilon_{xc}[n(r)]dr, \tag{1a}$$

$\varepsilon_{xc}[n(r)]$ is the one-particle functional of the exchange-correlation energy. This component is included in the effective Kohn and Sham potential by means of a one-particle equation:

$$\left\{ -\frac{1}{2}\nabla^2 + V_{eff}[n(r), r] \right\}\varphi_i(r) = \varepsilon_i\varphi_i(r), \tag{2a}$$

The DFT formalism proposed by Hohenberg, Kohn, and Sham [39,40] provides an effective description of the interaction between electrons and positrons. The expression for the positron wave function φ+(r) is given by:

$$n_+(r) = \sum_i \varphi_+(r)^2 \tag{3a}$$

The positron lifetime τ in an inhomogeneous electron gas was determined by means of the annihilation rate λ:

$$\lambda = \pi r_0^2 c \int dr n_+(r) n_-(r) \gamma = \pi r_0^2 c \sum_i \int dr. \tag{4}$$

Where: r_0 is the classical electron radius; c is the speed of light; and γ is the enhancement factor of the electron density at the positron. The precision of the iterative procedure is up to twelve decimal places.

3. Result and discussion

3.1. XRD analysis

Fig. 1 shows the X-ray diffraction patterns of unirradiated and irradiated nanopowdered TiC samples at different fluencies. TiC (FCC) has a cubic crystal structure and belongs to the Fm-3m space group [41]. The presence of TiC peaks at two-theta values of 36, 42, 61, 73, 77, 92, 103, and 107 indicates the formation of TiC. The absence of additional peaks suggests that the sample has been synthesized with high purity. On the other hand, no peak displacement or new peak formation was observed depending on the intensity of the neutron flux. The obtained peaks were indexed as face-centered (100), (110), (111), and (225), respectively. Additionally, the same XRD data were used in Rietveld refinement analysis based on a face-centered cubic structure, as shown in Fig. 1. The Ti and C elements were found to be coordinated at positions (0, 0, 2) and (1, 1, 0), respectively. As mentioned previously, Rietveld refinements were performed for the Fm-3m space group using similar initial parameters for the refinement models. After refining each parameter for different models, the reduction of Bragg R factor and χ2 values were lowered between 10 and 1 for goodness of the Rietveld refinement [42]. The refined parameters are presented in Table 2, and the lattice parameters and atomic planes were found to be fully consistent with previous literature results for nano TiC crystals [43–47]. It is worth noting that lattice parameters can vary between 4.20 Å and 4.33 Å depending on the stoichiometric ratio [47]. Our results show a slight deviation in lattice parameters within this range, with the unirradiated sample exhibiting a lattice parameter of 4.2888 Å. However, following neutron radiation at a fluence of 4.0×10^{12} n/cm^2, the lattice parameter increased to 4.2895 Å. For fluences of 1.3×10^{13} n/cm^2 and 4.0×10^{14} n/cm^2 doses, no significant changes were observed (it remained as if it was not irradiated). However, a decrease in the lattice parameter was observed at a fluence of 10^{15} n/cm^2. The lattice shrinkage is considered to result from the impact of higher energy irradiation, allowing for atomic annealing and increased crystallinity. This effect has been

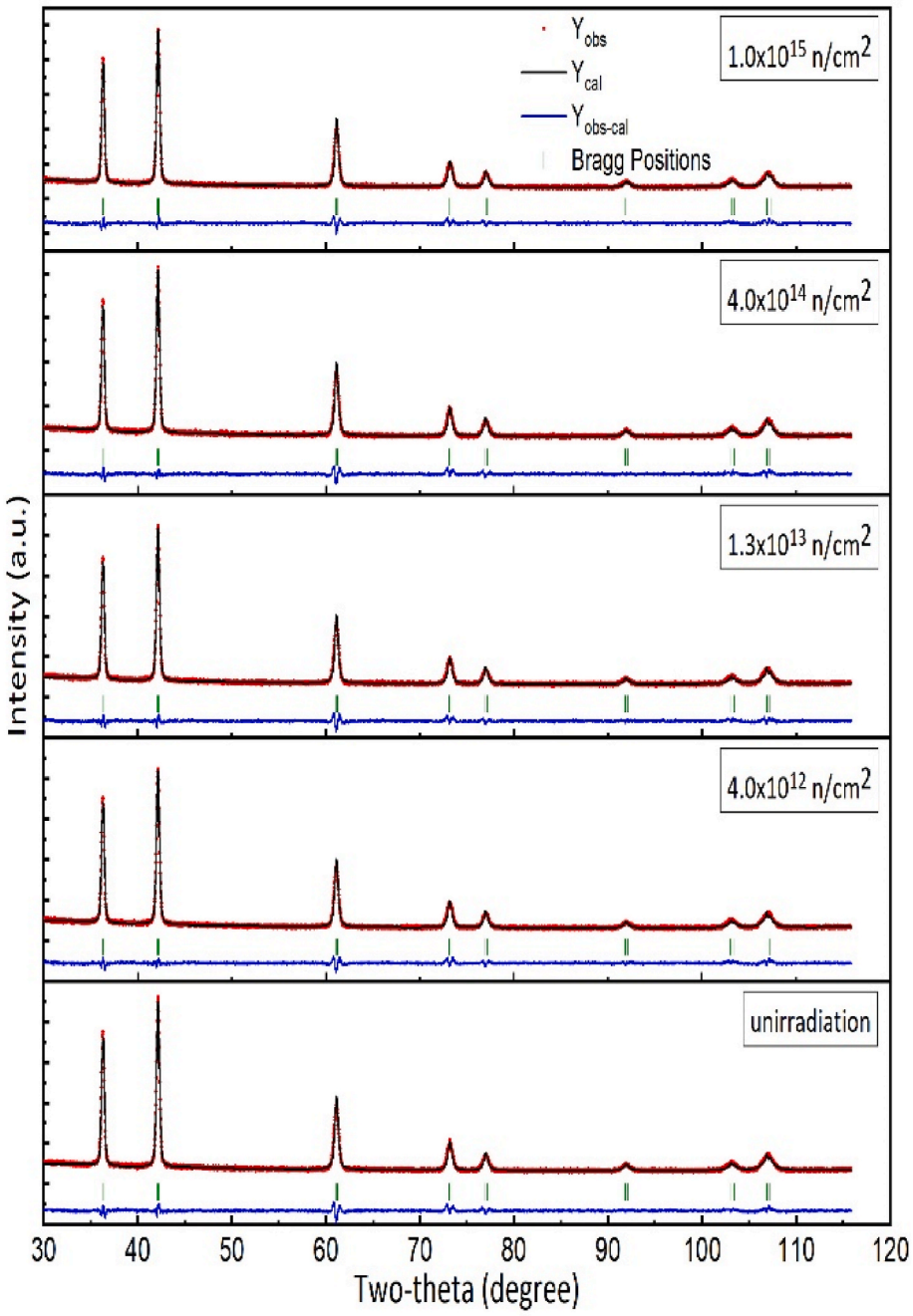

Fig. 1. X-ray diffraction patterns of unirradiated and irradiated at different fluencies nano powdered TiC samples.

Table 2
Rietveld refinement parameters for atomic lattice for different irradiation dose.

Neutron Irradiation (n/cm^2)	a(Å)	χ2	R Factor
Unirradiated	4.2888 (±0.00002)	2.24	1.73
4.0 × 10^{12}	4.2895 (±0.00002)	2.10	2.18
1.3 × 10^{13}	4.2889 (±0.00002)	2.15	1.97
4.0 × 10^{14}	4.2889 (±0.00002)	2.15	2.20
1.0 × 10^{15}	4.2876 (±0.00002)	2.26	1.98

previously reported [48], indicating consistency with our findings. The mechanism of defect formation and amorphization in the TiC crystal under the influence of fast neutrons is not observed.

3.2. Raman spectral analysis

At the nanoscale level, two types of processes are likely to occur in TiC samples - oxidation and amorphization. However, these processes are not easily detected using XRD, especially at small scales. While surface oxidation is a naturally occurring process that does not require irradiation, amorphization may only occur under irradiation. Although TiC lacks Raman-active modes due to its structure, any deviation from its stoichiometry can produce distinct Raman features in its spectra [49–55]. Therefore, Raman measurements were performed using a Helium–Neon laser with 633 nm excitation wavelength in the 50-2000 cm^{-1} range, and the collected spectra are presented in Fig. 2. Drawing on a range of previous studies focused on TiC [56–65], it can be inferred that identifying non-stoichiometric powdered TiC_{1-x} via Raman spectroscopy is feasible by detecting three distinct peaks that correspond to

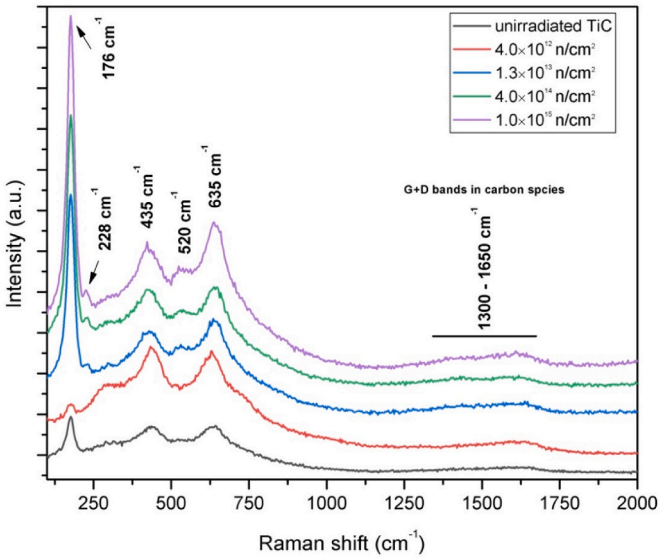

Fig. 2. Raman spectra of unirradiated TiC nanosized powder (bottom curve) and of irradiated at different fluencies samples.

the total vibrational $\Gamma = A_{1g} + E_g + T_{2g}$ of Raman-active modes [52]. These peaks are typically located at approximately 605 cm^{-1} for the A_{1g} mode, which ranges from 594 cm^{-1} to 623 cm^{-1} [50,52,56–59,61–66], 420 cm^{-1} for the E_g mode, ranging from 396 cm^{-1} to 426 cm^{-1} [50,52,56,58,59,61,62,64–66], and 260 cm^{-1} for the weakest peak intensity T_{2g} mode [52], which ranges from 250 cm^{-1} to 280 cm^{-1} [49,50,52,56–58,61–66]. Notably, the precise positioning of these peaks is independent of the excitation wavelength used for Raman probing (such as 512 nm, 532 nm or 633 nm) [57,60]. However, differentiating between surface oxidation products such as TiO_2 and TiC in a Raman spectrum can be challenging, as most of the unique TiO_2 Raman-active modes for both anatase and rutile polymorphs are found within a 30 cm^{-1} range surrounding the central positions of the TiC peaks [53,67–73]. Moreover, it should be noted that when TiC material is in the form of a single crystal, poly crystal, or thin film, the band positioning is entirely different, with four peaks or rather two doublets observed in the 280-700 cm^{-1} range [49,60,61,63]. The Raman spectrum of unirradiated TiC reveals four distinct spectral features, as demonstrated by the bottom curve in Fig. 2. At lower wave numbers, the spectrum displays a well-defined peak at 176 cm^{-1}, as well as two broad bands located at 435 cm^{-1} and 635 cm^{-1}, respectively. These latter two bands correspond to the E_g and A_{1g} modes of TiC_{1-x}, but shifted to higher wave numbers in comparison to previous reports [54,56]. The T_{2g} mode, which is another characteristic feature of non-stoichiometric TiC, is not prominently visible in this spectrum. It should be noted that rutile TiO_2 exhibits two strong Raman peaks at approximately 446 cm^{-1} and 610 cm^{-1}, respectively [53,67]. Given the susceptibility of TiC to oxidation, it is possible that the broad bands observed in the unirradiated spectrum may contain contributions from these characteristic rutile peaks. The peak at 176 cm^{-1} in the spectrum (Fig. 2) is the most intense and sharpest, and may be associated with the E_g Raman active mode of anatase TiO_2, albeit shifted to higher wave numbers than its authentic position at around 145 cm^{-1} [67,71–73].

This prominent peak at 176 cm^{-1} in the Raman spectrum may be associated with the E_g Raman active mode of anatase TiO_2 with a high degree of probability. However, it shifted to a higher wave number compared to its expected position at around 145 cm^{-1}, as reported in previous studies [67,71–73]. In this work, it could be inferred that samples subjected to irradiation at or above 1.3×10^{13} n/cm^2 exhibit a second anatase characteristic peak at 520 cm^{-1}, as observed in Fig. 2 [53,67,68,70–73]. Additionally, a new Raman feature emerging on the high-frequency shoulder of the 176 cm^{-1} peak increases in intensity with an increase in irradiation fluence, and it has been attributed to anatase TiO_2 [71–73].

The fourth Raman peak can be observed as a broad, ill-defined "bump" spanning from approximately 1300 cm^{-1} to 1650 cm^{-1} (Fig. 2). This spectral region contains the characteristic Raman bands for various graphitic materials, including the G-band at approximately 1330 cm^{-1} and the D-band at around 1620 cm^{-1}, which are well associated with the A_{1g} and E_{2g} vibrational modes, respectively [74,75]. The absence of these features in the Raman spectrum of unirradiated TiC indicates the near absence of non-reacted amorphous carbon in the nanosized powder. This provides evidence for good stoichiometry of the material with low carbon vacancies, which is also confirmed by the XRD results. Hence, the potential presence of non-stoichiometric TiC_{1-x} in the unirradiated TiC spectrum can be considered a minor contributor at best. It is highly likely that the primary contributor to the spectrum is a blend of oxidation products of anatase and rutile TiO_2. The low intensity and broadness of the Raman bands, coupled with the absence of well-crystallized second phase in the XRD data, suggest the presence of TiO_2 particles in very small sizes and quantities. The impact of irradiation on the material's characteristics can be observed in the TiC spectra at various fluencies, as depicted in Fig. 2. The spectrum of the sample irradiated at the lowest fluence (4.0×10^{12} n/cm^2) exhibits significant differences compared to both the original sample and those subjected to higher fluencies. The broad bands at 435 cm^{-1} and 635 cm^{-1} become narrower and markedly increase in intensity, while the peak associated with anatase TiO_2 at 176 cm^{-1} in the pristine sample nearly disappears. It is worth noting that this peak is attributed to the symmetric stretching vibrations of oxygen atoms in O–Ti–O bond [68,75]. Two new weak spectral features can be observed at approximately 290 cm^{-1} and 720 cm^{-1} in the TiC spectrum (Fig. 2). While there is a slight increase in intensity at the position of characteristic carbonaceous lines (1300 cm^{-1} to 1650 cm^{-1}), it is not significant enough to suggest the initiation of material amorphization. This is true even for samples irradiated at higher fluences, indicating that neutron irradiation does not lead to material amorphization, even at the highest fluence studied (10^{15} n/cm^2). These results are consistent with the findings of S. Pellegrino et al. [54,61], who used Au ions for TiC irradiation.

On the other hand, the spectrum exhibits a decrease in the intensity of the 176 cm^{-1} peak, accompanied by sharpening and an increase in the intensity of the peaks at 435 cm^{-1} and 635 cm^{-1} (Fig. 2). This phenomenon could be interpreted as a type of "surface healing" associated with deoxidation, leading to the presumable recovery of some of the Ti–C bonds at the surface. Supporting this hypothesis is the appearance of the low intensity features at 290 cm^{-1} and 720 cm^{-1} (Fig. 2). These are considered indications of the splitting of the peaks at 435 cm^{-1} and 635 cm^{-1}, respectively, into doublets, which is the principal spectral pattern observed for mono- and polycrystalline TiC samples [49,60,61,63]. The process of deoxidation can be easily observed in the Raman spectrum for anatase TiO_2, but not in the case of rutile TiO_2, as the peaks for both rutile and non-stoichiometric TiC overlap. It is likely that the deoxidation process affects both polymorphic forms of TiO_2, given that neutron irradiation is known to induce intrinsic defect states, such as oxygen vacancies in rutile [76–79]. As previously noted, the spectra of TiC samples irradiated at fluencies of 1.3×10^{13} n/cm^2, 4.0×10^{14} n/cm^2, and 10^{15} n/cm^2 exhibit similarities (Fig. 2). All spectra display a highly intense peak at 176 cm^{-1} with a small peak at 225 cm^{-1} on its high frequency shoulder, as well as a new band at 520 cm^{-1}. These features suggest a significant increase in the contribution of anatase phase to TiC_{1-x} spectrum. This reconstruction of Ti–O bonds with increasing irradiation fluence indicates that a TiO_2 consolidation effect likely takes place on the surface of the TiC particles. This is further supported by the increase in intensity of all anatase-assigned peaks and the appearance of the peak at 225 cm^{-1}, which is characteristic of particles of anatase above a certain size [71]. Furthermore, the non-monotonic nature of the observed changes with increasing irradiation dose is worth noting, which it is also consistent with the

observations of TiC by Pellegrinno et al. [61].

3.3. Fourier transform infrared (FTIR) spectroscopy

The results showed in Fig. 3 illustrate the Fourier transform infrared (FTIR) spectra of nano TiC crystals exposed to fast neutrons with varying intensities of 1 MeV energy. The non-irradiated and irradiated nano TiC crystals up to 10^{15} n/cm^2 intensity displayed peaks indicative of distinct modes. Notably, the 645 cm^{-1} T-C vibration modes [80], 745 cm-1 O=Ti=O modes, and 841 cm^{-1} modes [81] were detected. Furthermore, the 1066 cm^{-1} TiC surface exhibited =C=O radicals associated with vibration modes. In the wavenumber range of 1000–1500 cm-1, the spectral features corresponding to weak interactions of the functional groups =C–H and =C=O are typically observed [82,83]. Additionally, the interval from 2900 to 3450 cm^{-1} is known to correspond to the valence v (OH) oscillations of water molecules adsorbed on the surface of the crystal [84]. After irradiation, a decrease in the spectral peaks attributed to absorbed water can be observed (Fig. 3). The underlying mechanism for the decomposition of absorbed water molecules under the influence of different neutron fluxes can be explained through the following diagrams.

$$H–OH + TiO_2 \leftrightarrow Ti–OH_2^+ + (=C=O) \quad (1b)$$

$$Ti–OH \leftrightarrow Ti–O + H^+ \quad (2b)$$

$$Ti–OH_2^+ \leftrightarrow Ti–OH + H^+ \quad (3b)$$

A comparison of the Raman and FTIR analyses reveals an increase in the intensity of modes that characterize the chemical bond O=Ti=O, indicating the formation of TiO_2 crystal centers as a result of reactions with mechanism (2).

3.4. Surface morphology analysis

The images of nano-sized crystal TiC before and after irradiation with different neutron fluxes obtained using TEM and SEAD methods were presented in Fig. 4 and Fig. 5. The results of Raman and FTIR analysis indicate that the nano TiC crystals do not undergo amorphization depending on irradiation. Furthermore, TEM images reveal that the crystal size ranges from 50 to 120 nm and remains unchanged depending on the intensity of the neutron flux. This funding is also supported by the Raman analysis, which confirms that the crystallite size remains constant. Additionally, SEAD micrographs provide information on the structural properties of TiC, which exhibits a halite structure type with cubic symmetry (space group-Fm3m), cage parameters of 4.3280 A^o, a cage volume of 81.67 A^3, and a molar volume of 12.21 cm^3/mol. The experiments revealed that changes in the interatomic planes (200, 111, 220, 113 and 222) of the nano TiC crystal were observed depending on the intensity of radiation. However, the maximum intensity of the (200) plane remained unaffected. The experimental results from all analyses showed that irradiation of the nano-crystalline TiC sample with fast neutrons with an energy of 0.1 MeV up to 10^{15} n/cm^2 did not lead to any structural damage and the crystal maintained a stable structure.

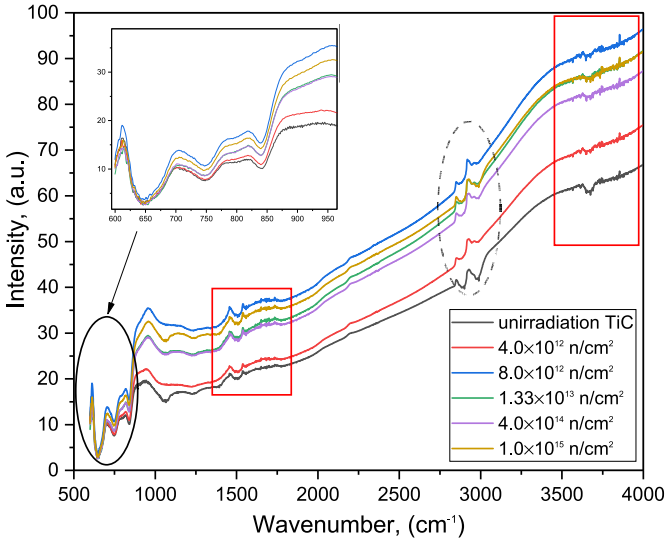

Fig. 3. FTIR spectroscopy of nano TiC crystal at different neutron irradiation fluencies.

3.5. PLT calculations

A structure consisting of 500 TiC molecules was utilized to construct the TiC lattice in MIKA. The void cluster was increased to 2 vacancies, specifically a di-vacancy consisting of 1 Ti and 1 C atom. The distribution of hydrogen (H) and helium (He) atoms within the void clusters was gradually increased, considering the potential formation of hydrogen molecules as well as the likelihood of valence interaction between hydrogen and neighboring atoms of the underlying material. Based on the fact that hydrogen molecules have stronger molecular bonds than hydride modifications at Ti and C, it is anticipated that hydrogen-hydrogen interactions will be the primary interaction in vacancies [85–87]. The MIKA calculation was conducted without relaxation, but the H and He atoms were relocated to positions that could be occupied due to Ti–H or C–H chemical bonds [88,89]. For test calculations, a different type of Ti structure was utilized as a starting point. In Fig. 6, a cluster consisting of two vacancies is depicted with 4H and 4He atoms implanted. The calculated values of τ are listed in Table 3 and presented graphically in Fig. 6. The graph in Fig. 7 illustrates the correlation between the number of implanted H or He atoms and the corresponding values of τ, as presented in Table 3. TiC, similar to WC, can be considered as a layered material that exhibits strong metallic properties while possessing a two-dimensional structure consisting of a light element. In order to make a comparison, fcc Ti was used as a benchmark, although evaluations were also conducted on bcc and xec Ti. The resulting data suggests that the variations observed are negligible and can be attributed to potential deformations in the lattice constants [90]. In TiC materials, the positron lifetime by calculation was 111.9 ps. However, the presence of a single TiC vacancy in the crystal structure of TiC increases this time to 180.1 ps. On the other hand, when a C vacancy replaces a Ti vacancy, the difference in positron lifetime values between the perfect lattice and the vacancy-containing structure decreases. The data presented in Table 1 demonstrate that the τ value increases at a faster rate for a Ti vacancy compared to a C vacancy. This observation is reasonable since the volume of the titanium atom is considerably larger than that of the carbon atom, although the valence electrons are equal in both cases. The electron density in a titanium vacancy is significantly lower than in a carbon vacancy, although the positron lifetime is functionally dependent on the electron density. Based on the observed range of values for different types of defects in Ti and TiC, it can be inferred that TiC is a better material as compared to Ti. The difference between τ for a titanium vacancy and a perfect lattice (bulk) in Ti is 88 ps, while in TiC, it is approximately 68 ps. Additionally, the layered structure of TiC makes it a promising candidate for use in radiation protection from ion radiation. This inference is further supported by the “trampoline effect,” a phenomenon resulting from the irradiation of two-dimensional structures of nano-particles, as described in reference [91]. To establish a reliable benchmark, a comparison was made with the results obtained by Gopalan [92]. The study by Gopalan provided a result for a perfect lattice that matched our findings. On the other hand, De Vries reported lifetime values around 160 ps, which depended on annealing conditions and temperature kinetics, suggesting the possibility of a non-stoichiometric form of the material being considered. The results in our Table 3 that were closest to this value were observed for implantation. Therefore, it is plausible to assume that non-stoichiometry may be

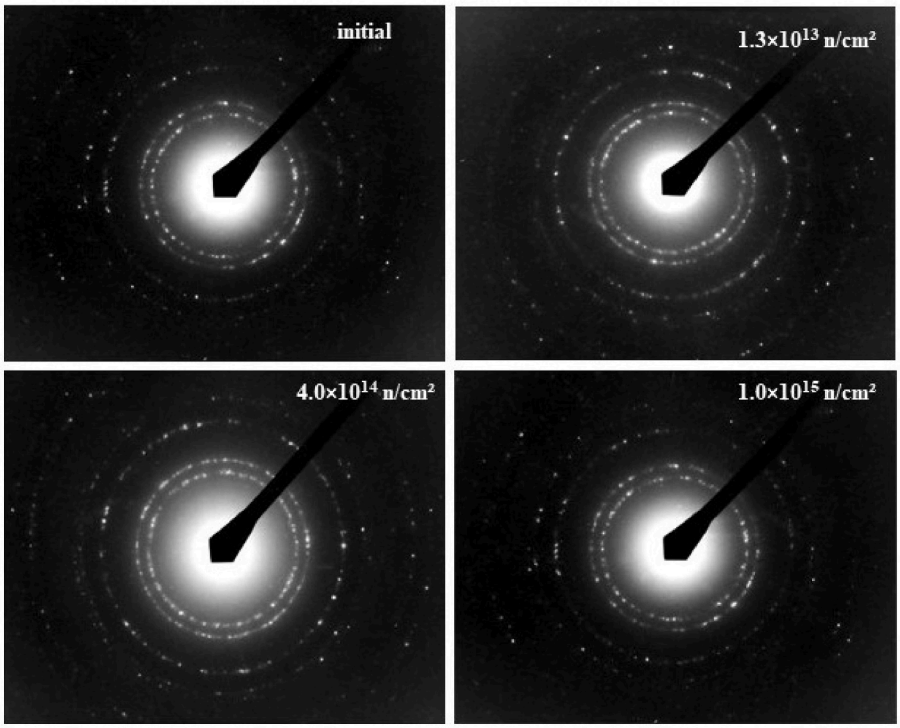

Fig. 4. SAED patterns of nano titanium carbide sample at different neutron irradiation fluencies.

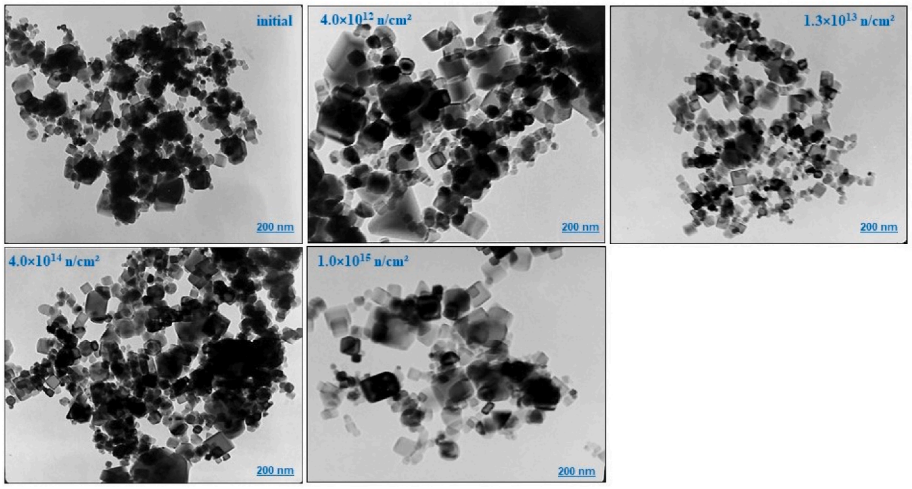

Fig. 5. TEM images patterns of nano titanium carbide sample at different neutron irradiation fluencies.

present in De Vries samples. In Fig. 6, the positron lifetime (τ) is presented as a function of the number of implanted hydrogen or helium atoms. The observed decrease in τ values can be attributed to the increased electron density caused by the impurity atoms, which in turn reduces the effective size of the vacancy cluster. Notably, the τ values for $1Ti_V + nHe$ decrease more rapidly than those for $1Ti_V + nH$ due to the presence of an additional electron in the helium atom's outer shell. Although both electrons of the helium atom are in a bound state, they occupy the same 1 S orbital, making annihilation with them highly likely. A similar trend in τ values is observed for $1C_V + nH$ and $1C_V + nHe$. One of the noteworthy observations in Fig. 6 is the saturation of $1C_V$ with hydrogen, which exhibits an unconventional curve shape and a sharp decrease in τ values as the number of hydrogen atoms increases from one to two. This behavior can be attributed to the distinct chemical interactions between the hydrogen electrons and the vacancy. Furthermore, the comparison of the τ change upon saturation of a titanium vacancy with hydrogen and helium for both TiC and Ti corroborates our previous conclusion that TiC is a more stable material. This conclusion is reiterated by an analogous comparison between the results of a di-vacancy for TiC with one vacancy for Ti. Specifically, the difference from 0 impurities atoms in the di-vacancy to 4 hydrogen atoms is 63.5 ps, whereas the difference from 1 vacancy in Ti to 4 hydrogen atoms is 83.8 ps. Thus, we can again claim that TiC material has significantly better density qualities and, accordingly, resistance to ion radiation than Ti. The smoother course of the curves for the saturated vacancy clusters with implanted hydrogen and helium atoms at TiC compared to the analogous curves at Ti in Fig. 6 supports this interpretation. In the present work, the main claim can be made that TiC, which has a sufficiently high melting temperature of 3160 °C, can be considered as a competitor to tungsten for use as a diverter coating in a

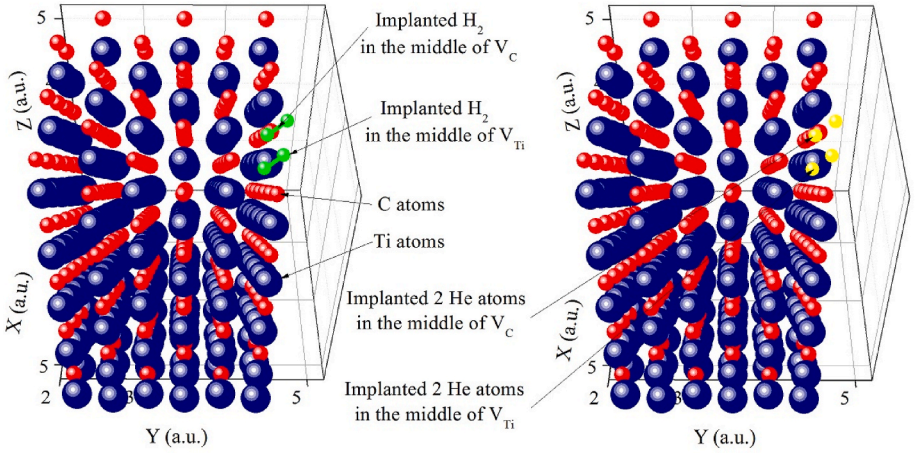

Fig. 6. Vacancy cluster formed by two vacancies (1Ti vacancy and 1C vacancy) where 4H or 4He atoms were implanted.

Table 3
Values of τ depending from number of vacancies in vacancy cluster and impurities H and He atoms in structure TiC and $Ti_{(fcc,\ xec,\ bcc)}$.

No. V_{Ti}	No. V_C	No. imp H	No. imp He	τ(ps)/ TiC	τ(ps)/ Ti_{fcc}	τ(ps)/ Ti_{xec}	τ(ps)/ Ti_{bcc}
–	–	–	–	111.9	147.7	148.9	147.9
1	–	–	–	180.1	235.7	235.3	236.2
–	1	–	–	139			
1	1	–	–	198.2			
1	–	1	–	159.6	205		
1	–	2	–	138.5	176.7		
1	–	4	–	118.6	151.9		
–	1	1	–	137.6			
–	1	2	–	112.3			
1	1	1	–	179.2			
1	1	2	–	159.2			
1	1	4	–	134.7			
1	–	–	1	133.7	175.9		
1	–	–	2	119.2	154.9		
–	1	–	1	115.4			
1	1	–	1	158.8			
1	1	–	2	140.2			
1	1	–	4	118.4			

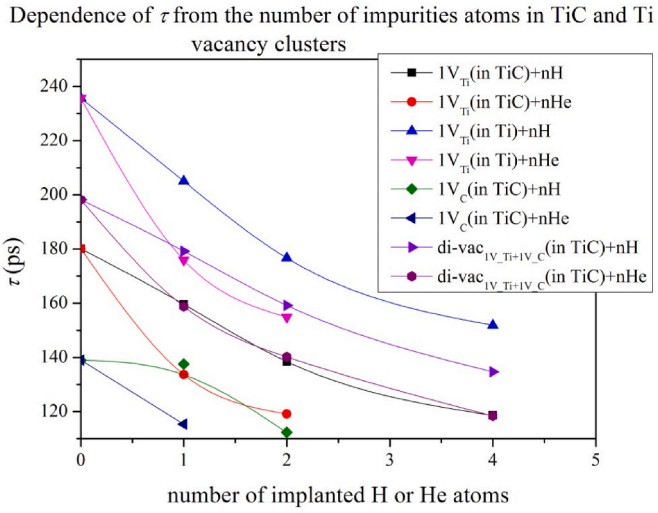

Fig. 7. Variation of τ for the implanted H or He atoms in vacancy clusters from one, two vacancies by TiC and in 1 vacancy by Ti.

fusion reactor. Despite its lower atomic number and corresponding atomic weight, TiC exhibits good radiation resistance, making it a promising candidate for this application. Moreover, TiC offers the additional advantage of producing low activity daughter isotopes.

4. Conclusions

In conclusion, the investigation of the effects of fast neutron irradiation on nano TiC crystals revealed that the crystals remained structurally stable up to 10^{15} n/cm^2 intensity of radiation. The Raman and FTIR analyses revealed an increase in the intensity of modes associated with the chemical bond O=Ti=O, which suggests the generation of TiO_2 crystal centers. Structural analyses revealed that TiC exhibited a halite structure type with cubic symmetry, and changes in the interatomic planes of the nano TiC crystal were observed depending on the intensity of radiation. X-ray diffraction (XRD) analysis revealed an annealing effect with increasing neutron dose, which is consistent with the observed increase in the anatase phase relative to rutile for TiO_2 on the surface as demonstrated by Raman and FTIR results. The consolidation of TiO_2 occurred on the grain surface, and these observations are consistent with the non-monotonic nature of the TiO_2 phase change. The results of the PLT indicate that TiC is a better material for radiation protection than Ti due to its strong metallic properties and two-dimensional structure, as determined by the MIKA software. Moreover, it can be concluded that hydrogen-hydrogen interactions are the primary interaction in vacancies, and the electron density in a titanium vacancy is considerably lower than in a carbon vacancy. The morphological analysis by transmission electron microscopy (TEM) and selected area electron diffraction (SEAD) confirmed the material's exceptional structural stability to neutron irradiation without amorphization. Additionally, our model calculations for implanting hydrogen and helium atoms into a TiC sample are consistent with the findings and the results suggest that the nano TiC crystals can withstand fast neutron irradiation without any significant structural damage, making them suitable for various applications in radiation environments.

CRediT authorship contribution statement

E. Popov: Writing – review & editing, Investigation. **L. Slavov:** Writing – review & editing, Visualization, Methodology. **E. Demir:** Software, Methodology. **B.A. Abdurakhimov:** Software, Investigation, Conceptualization. **A.S. Doroshkevich:** Visualization, Methodology, Investigation. **O.A. Aliyev:** Visualization, Software, Methodology. **S.H. Jabarov:** Methodology, Investigation. **A.H. Valizade:** Supervision, Methodology. **B. Mauyey:** Validation, Software. **P. Horodek:** Writing – review & editing. **K. Siemek:** Writing – review & editing. **O. Samedov:**

Writing – review & editing. **M.N. Mirzayev:** Writing – review & editing, Writing – original draft, Project administration, Methodology.

Declaration of competing interest

The authors declare that they have no known competing financial interests or personal relationships that could have appeared to influence the work reported in this paper.

Data availability

No data was used for the research described in the article.

Acknowledgments

This work was supported by the Azerbaijan Science Foundation-Grant N№ AEF-MCG-2022-1(42)-12/03/1-M-03

References

[1] S. Agarwal, T. Koyanagi, A. Bhattacharya, L. Wang, Y. Katoh, X. Hu, M. Pagan, S. J. Zinkle, Neutron irradiation-induced microstructure damage in ultra-high temperature ceramic TiC, Actamaterialia186 (2020) 1–10.
[2] T. Chen, M. Li, S. Song, P. Kim, J. Bae, Biotemplate preparation of multilayered TiCnanoflakes for high performance symmetric supercapacitor, Nano Energy 71 (2020), 104549.
[3] M. Mhadhbi, M. Driss, Titanium carbide: synthesis, properties, application, Journal of Brilliant Engineering 2 (2021) 1–11, https://doi.org/10.36937/ben.2021.002.001.
[4] M. Jiang, J.W. Zheng, H.Y. Xiao, Z.J. Liu, X.T. Zu, A Comparative Study of the Mechanical and Thermal Properties of Defective ZrC, TiC and SiC, Scientific Reports7, 2017, pp. 1–14.
[5] M. Jiang, H.Y. Xiao, H.B. Zhang, S.M. Peng, C.H. Xu, Z.J. Liu, X.T. Zu, A Comparative Study of Low Energy Radiation Responses of SiC, TiC and ZrC, ActaMaterialia110, 2016, pp. 192–199.
[6] Y. Tan, Z. Teng, P. Jia, X. Zhou, H. Zhang, Diverse Oxidation Behaviors of Metal Carbide Solutions in High-Temperature Water Vapor, Corrosion Science191, 2021, 109758.
[7] M. Azadi, A.S. Rouhaghdam, S. Ahangarani, H.H. Mofidi, M. Valiei, Mechanical behavior and properties of TiN/TiC coating using PACVD, Advanced Materials Research, Trans. Tech. Publ. 829 (2014) 476–481. 10.4028/www.scientific.net/amr.829.476.
[8] H. Mofidi, A.S.R. Aghdam, S. Ahangarani, M. Bozorg, M. Azadi, M. Valiei, Deposition of titanium layer on steel substrate using pecvd method: a parametric study, Mater. Sci. Appl. 5 (3) (2014) 1–9, https://doi.org/10.4236/msa.2014.53018.
[9] S.T. Oyama, Introduction to the Chemistry of Transition Metal Carbides and Nitrides, 1996, https://doi.org/10.1007/978-94-009-1565-7_1.
[10] S.A. Rasaki, B. Zhang, K. Anbalgam, T. Thomas, M. Yang, Synthesis and application of nano-structured metal nitrides and carbides: a review, Prog. Solid State Chem. 50 (2018) 1–15, https://doi.org/10.1016/j.progsolidstchem.2018.05.001.
[11] Y. Tan, W. Liao, Y. Xia, Z. Teng, P. Jia, X. Zhou, H. Zhang, Understanding the Oxidation Kinetics of (Ti0.8Nb0.2)C and (Ti0.8Nb0.2)C-SiC Composite in High-Temperature Water Vapor, Corrosion Science200, 2022, 110248.
[12] M.T. Lusk, A.E. Mattsson, High-performance computing for materials design to advance energy science, MRS Bull. 36 (2011) 216–222.
[13] Yu Dan, Y. Tan, Evolution of the Oxidation Behaviors of Highly Oxidation-Resistant (Ti0.8Nb0.2)C in 1000–1200° C Steam, RSC advances12, 2022, pp. 20492–20498.
[14] T.R. Allen, K. Sridharan, L. Tan, W.E. Windes, J.I. Cole, D.C. Crawford, G.S. Was, Materials challenges for generation IV nuclear energy systems, Nucl. Technol. 162 (2008) 342–357, https://doi.org/10.13182/NT08-A3961.
[15] J.X. Xue, J.X. Liu, G.J. Zhang, H.B. Zhang, T. Liu, X.S. Zhou, S.M. Peng, Improvement in Mechanical/physical Properties of TiC-Based Ceramics Sintered at 1500 C for Inert Matrix fuels,ScriptaMaterialia, 114, 2016, pp. 5–8.
[16] D. Neov, L. Slavov, A.A. Donkov, M.N. Mirzayev, E. Popov, E. Demir, K. Siemek, N. Djourelov, V.A. Turchenko, Z.A. Sharipov, P. Horodek, Structural study of W_2B obtained via mechanical alloying of W, B_4C, TiC and graphite before and after He ions irradiation, Nuclear Materials and Energy 31 (2022), 101201.
[17] M.S. Koval'chenko, V.V. Ogorodnikov, A.G. Krainii, Effect of Neutron Irradiation on the Structure and Properties of Lanthanum Hexaboride, Soviet Atomic Energy21, 1966, pp. 1168–1174.
[18] G.W. Keilholtz, R.E. Moore, M.F. Osborne, Fast-neutron effects on the carbides of titanium, zirconium, tantalum, niobium, and tungsten, Nucl. Appl. 4 (1968) 330–336.
[19] M.S. Koval'chenko, V.V. Ogorodnikov, A.G. Krainii, L.F. Ochkas, The Effect of Neutron Irradiation on the Structure of Titanium and Chromium Carbides, Refractory Carbides, Springer, New York, 1974, pp. 209–220.
[20] J. Morillo, C.H. de Novion, J. Dural, Neutron and electron radiation defects in titanium and tantalum monocarbides: an electrical resistivity study, Radiat. Eff. 55 (1981) 67–77.
[21] H. Matsui, M.W. Guinan, T. Iida, M. Iseki, Fusion neutron irradiation of TiC, J. Nucl. Mater. 133 (1985) 718–721.
[22] H. Matsui, M. Iseki, Fast neutron damage in TiC_{1-x}, J. Nucl. Mater. 152 (1988) 14–20.
[23] H. Matsui, K. Nesaki, M. Kiritani, Neutron irradiation damage in transition metal carbides, Journal of Nuclear Materials179 (1991) 461–464.
[24] M.S. Koval'chenko, YuI. Rogovoi, V.D. Kelim, Change in the Structure and Properties of Titanium Carbide under the Action of Irradiation, Soviet Atomic Energy32, 1972, pp. 362–364.
[25] J. Kuriplach, Principles of positron annihilation and positron response calculations, in: Joint ICTP-IAEA Advanced Workshop on Multi-Scale Modellin G for Characterization and Basic Understanding of Radiation Damage Mechanisms in Materials, ICTP, Trieste, Italy, 2010.
[26] J. Dryzek, Positron trapping model in fine grained sample, Acta Phys. Pol., A 95 (1999) 125–129.
[27] M.N. Mirzayev, Simultaneous measurements of heat flow rate and thermal properties of nano boron trioxide under neutron irradiation at the low and high temperature, Vacuum 173 (2020), 109162.
[28] M.N. Mirzayev, Heat transfer of hexagonal boron nitride (h-BN) compound up to 1 MeV neutron energy: kinetics of the release of wigner energy, Radiat. Phys. Chem. 180 (2021), 109244.
[29] M.N. Mirzayev, B.A. Abdurakhimov, E. Demir, A.A. Donkov, E. Popov, M. Yu Tashmetov, I.G. Genov, T.T. Thabethe, K. Siemek, K. Krezhov, F. Mamedov, D. M. Mirzayeva, M.V. Bulavin, V.A. Turchenko, T.X. Thang, T.Z. Abdurakhmonov, P. Horodek, Investigation of the formation of defects under fast neutrons and gamma irradiationin 3C-SiC nano powder, Phys. B Condens. Matter 611 (2021), 412842.
[30] M.N. Mirzayev, High-flux neutron irradiation of boron trioxide analyzed with Raman and FTIR spectroscopy, Int. J. Mod. Phys. B 34 (18) (2020), 2050160.
[31] Y.G. Dragunov, I.T. Tretiyakov, A.V. Lopatkin, N.V. Romanova, I.B. Lukasevich, V. D. Ananyev, A.V. Vinogradov, A.V. Dolgikh, L.V. Yedunov, Y.N. Pepelyshev, A. D. Rogov, E.P. Shabalin, A.A. Zaikin, I.S. Golovnin, Modernization of the IBR-2 pulsed research reactor, At. Energy. 113 (2012) 29–38.
[32] A.P. Cheplakov, V.V. Golikov, S.M. Golubyh, G.Y. Kaskanov, E.N. Kulagin, V. V. Kukhti, V.I. Luschikov, E.P. Shabalin, E. León-Florián, C. Leroy, Large-scale samples irradiation facility at the IBR-2 reactor in Dubna, Nucl. Instruments Methods Phys. Res. Sect. A Accel. Spectrometers, Detect. Assoc. Equip. 411 (1998) 330–338.
[33] E. Demir, M.N. Mirzayev, E.P. Popov, P. Horodek, I.G. Genov, K. Siemek, D. M. Mirzayeva, V.A. Turchenko, M. Bulavin, A.I. Beskrovnyi, A.H. Valizade, H. V. Akhundzada, S.I. Karaaslan, Effects of high-energetic $^3He^+$ ion irradiation on tungsten-based composites, Vacuum 184 (2021), 109934.
[34] E. Demir, M.N. Mirzayev, A.B. Tuğrul, B.A. Abdurakhimov, S.I. Karaaslan, An experimental study on microstructure of tungsten alloys, Surf. Rev. Lett. 27 (7) (2020), 1950169.
[35] A. Olejniczak, N.A. Nebogatikova, A.V. Frolov, M. Kulik, I.V. Antonova, V. A. Skuratov, Swift heavy-ion irradiation of graphene oxide: localized reduction and formation of sp-hybridized carbon chains, Carbon 141 (2019) 390–399.
[36] I. Makkonen, M. Hakala, M.J. Puska, Modeling the momentum distributions of annihilating electron-positron pairs in solids, Phys. Rev. B 73 (2006), 035103.
[37] https://materialsproject.org/materials/mp-631.
[38] E. Boronski, R.M. Nieminen, Electron-positrondensity-functional theory, Phys. Rev. B 34 (1986) 3820.
[39] P. Hohenberg, W. Kohn, Homogeneous electron gas, Phys. Rev. 136 (1964) B864.
[40] W. Kohn, L.J. Sham, Self-consistent equations including exchange and correlation effects, Phys. Rev. 140 (4A) (1965) A1133.
[41] B.-X. Dong, F. Qiu, Q. Li, S.-L. Shu, H.-Y. Yang, Q.-C. Jiang, The synthesis, structure, morphology characterizations and evolution mechanisms of nanosized titanium carbides and their, further applications, Nanomaterials 9 (2019) 1152.
[42] L.B. McCusker, R.B. Von Dreele, D.E. Cox, D. Louër, P. Scardi, Rietveld refinement guidelines, J. Appl. Crystallogr. 32 (1999) 36–50.
[43] C. Xu, K. Bao, S. Ma, D. Li, D. Duan, H. Yu, X. Jin, F. Tian, B. Liu, T. Cui, Revealing unusual rigid diamond net analogues insuperhard titanium carbides, RSC Adv. 8 (2018), 14479.
[44] S.B. Jin, P. Shen, Q.L. Lin, L. Zhan, Q.C. Jiang, Growth mechanism of TiC_x during self-propagating high-temperature synthesis in an Al-Ti-C System, Cryst. Growth Des. 10 (2010) 1590–1597.
[45] Z. Wang, J.W. Sun, Y.H. Cheng, C.M. Niu, Adsorption and deposition of Li_2O_2 on TiC {111} surface, J. Phys. Chem. Lett. 5 (2014) 3919–3923.
[46] B.W. Davis, R.G. Varsanik, A study of crystalline titanium carbide, J. Colloid Interface Sci. 37 (1971) 870–878.
[47] B. Jiang, N. Hou, S. Huang, G. Zhou, J. Hou, Z. Cao, H. Zhu, Structural studies of $TiC_{1-x}O_x$ solid solution by Rietveld refinement and first-principles calculations, J. Solid State Chem. 204 (2013) 1–8.
[48] E. Demir, E. Popov, M. Mirzayev, L. Slavov, D. Neov, A. Donkov, K. Siemek, T. Vershinina, I. Genov, A. Beskrovnyi, V. Skuratov, K. Krezhov, P. Horodek, F. Mamedov, A. Valizade, O. Vural, Effects of swift heavy ions at different fluencies on WC-6Co hard metal alloy, Int. J. Refract. Metals Hard Mater. 106 (2022), 105865.
[49] M.V. Klein, J.A. Holy, W.S. Williams, Raman scattering induced by carbon vacancies in TiC_x, Phys. Rev. B 17 (1978) 1546–1556.
[50] L. Aihaiti, K. Tuokedaerhan, B. Sadeh, M. Zhang, X. Shen, A. Mijiti, Effect of annealing temperature on microstructure and resistivity of TiC thin films, Coatings 11 (4) (2021) 457.
[51] N. Kumar, G. Natarajan, R. Dumpala, R. Pandian, A. Bahuguna, S.K. Srivastava, T. R. Ravindran, S. Rajagopalan, S. Dash, A.K. Tyagi, M.R. Rao, Microstructure and

phase composition dependent tribological properties of TiC/a-C nanocomposite thin films, Surf. Coating. Technol. 258 (2014) 557–565.
[52] J.E. Oghenevweta, D. Wexler, A. Calka, Study of reaction sequences during MSR synthesis of TiC by controlled ball milling of titanium and graphite, Mater. Char. 140 (2018) 299–311.
[53] J.C. Sánchez-López, D. Martínez-Martínez, C. López-Cartes, A. Fernández, Tribological behaviour of titanium carbide/amorphous carbon nanocomposite coatings: from macro to the micro-scale, Surf. Coating. Technol. 202 (2008) 4011–4018.
[54] S. Pellegrino, L. Thomé, A. Debelle, S. Miro, P. Trocellier, Radiation effects in carbides: TiC and ZrC versus SiC, Nucl. Instrum. Methods Phys. Res. Sect. B Beam Interact. Mater. Atoms 327 (2014) 103–107.
[55] M. Hassan, R.S. Rawat, P. Lee, S.M. Hassan, A. Qayyum, R. Ahmad, G. Murtaza, M. Zakaullah, Synthesis of nanocrystalline multiphase titanium oxycarbide (TiC_xO_y) thin films by UNU/ICTP and NX2 plasma focus devices, Appl. Phys. A 90 (2008) 669–677.
[56] Y.K. Kim, J.P. Kim, C.K. Park, S.J. Yun, W. Kim, S. Heu, J.S. Park, Electron-emission properties of titanium carbide-coated carbon nanotubes grown on a nano-sized tungsten tip, Thin Solid Films 517 (2008) 1156–1160.
[57] X.H. Gao, Z.M. Guo, Q.F. Geng, P.J. Ma, G. Liu, Structure, optical properties and thermal stability of TiC-based tandem spectrally selective solar absorber coating, Sol. Energy Mater. Sol. Cell. 157 (2016) 543–549.
[58] F. Huang, S. Fan, Y. Tian, X. Qu, X. Li, M. Javid, X. Zhang, Z. Zhang, X. Dong, Regulation of structural and terahertz properties of TiC nanoparticles by carbon-coating and N-doping, J. Phys. Chem. Solid. 169 (2022), 110825.
[59] T. Chen, M. Li, S. Song, P. Kim, J. Bae, Biotemplate preparation of multi-layered TiC nano flakes for high performance symmetric supercapacitor, Nano Energy 71 (2020), 104549.
[60] A.Z.A. Djafer, N. Saoula, N. Madaoui, A. Zerizer, Deposition and characterization of titanium carbide thin films by magnetron sputtering using Ti and TiC targets, Appl. Surf. Sci. 312 (2014) 57–62.
[61] S. Pellegrino, P. Trocellier, L. Thomé, S. Miro, J.M. Costantini, E. Jouanny, Raman investigation of ion irradiated TiC and ZrC, Nucl. Instrum. Methods Phys. Res. Sect. B Beam Interact. Mater. Atoms 454 (2019) 61–67.
[62] M. Lou, X. Chen, K. Xu, Z. Deng, L. Chen, J. Lv, K. Chang, L. Wang, Temperature-induced wear transition in ceramic-metal composites, Acta Mater. 205 (2021), 116545.
[63] Q. Qi, W.Z. Zhang, L.Q. Shi, W.Y. Zhang, W. Zhang, B. Zhang, Preparation of single-crystal TiC (111) by radio frequency magnetron sputtering at low temperature, Thin Solid Films 520 (2012) 6882–6887.
[64] B.H. Lohse, A. Calka, D. Wexler, Raman spectroscopy as a tool to study TiC formation during controlled ball milling, J. Appl. Phys. 97 (2005), 114912.
[65] K.S. Munir, Y. Zheng, D. Zhang, J. Lin, Y. Li, C. Wen, Improving the strengthening efficiency of carbon nanotubes in titanium metal matrix composites, Mater. Sci. Eng. A 696 (2017) 10–25.
[66] X. Yuan, L. Cheng, L. Kong, X. Yin, L. Zhang, Preparation of titanium carbide nanowires for application in electromagnetic wave absorption, J. Alloys Compd. 596 (2014) 132–139.
[67] J.G. Li, T. Ishigaki, X. Sun, Anatase, brookite, and rutile nanocrystals via redox reactions under mild hydrothermal conditions: phase-selective synthesis and physicochemical properties, J. Phys. Chem. C 111 (2007) 4969–4976.
[68] H. Rafik, M. Izerrouken, Radiation damage induced by reactor neutrons in nano-anatase TiO2 thin film, Radiat. Phys. Chem. 177 (2020), 109114.
[69] Z. Lu, Q. Zhou, Y. Ling, B. Hou, J. Wang, Z. Zhang, Preparation and hydrogen penetration performance of TiO_2/TiC_x composite coatings, Int. J. Hydrogen Energy 45 (2020) 14048–14061.
[70] M.J. Šćepanović, M. Grujić-Brojčin, Z.D. Dohčević-Mitrović, Z.V. Popović, Characterization of anatase TiO_2 nanopowder by variable-temperature Raman spectroscopy, Sci. Sinter. 41 (2009) 67–73.
[71] M.N. Mirzayev, L. Slavov, A. Donkov, D. Neov, E. Popov, E. Demir, I. Genov, B. Abdurakhimov, A. Vladescu, S. Biira, T. Karaman, Effects of neutron irradiation at different fluencies on nano sized anatase titanium dioxide, Radiat. Phys. Chem. 194 (2022), 109988.
[72] X. Chen, S.S. Mao, Titanium dioxide nanomaterials: synthesis, properties, modifications, and applications, Chem. Rev. 107 (2007) 2891–2959.
[73] W. Ma, Z. Lu, M. Zhang, Investigation of structural transformations in nanophase titanium dioxide by Raman spectroscopy, Appl. Phys. A 66 (1998) 621–627.
[74] A. Ferrari, J. Robertson, Interpretation of Raman spectra of disordered and amorphous carbon, Phys. Rev. 61 (2000) 14095–14107.
[75] D.A. Ferrari, D. Basko, Raman spectroscopy as a versatile tool for studying the properties of graphene, Nat. Nanotechnol. 8 (2013) 235–246.
[76] S.A. Abdullah, M.Z. Sahdan, N. Nayan, Z. Embong, C.R.C. Hak, F. Adriyanto, Neutron beam interaction with rutile TiO_2 single crystal (111): Raman and XPS study on Ti^{3+}-oxygen vacancy formation, Mater. Lett. 263 (2020), 127143.
[77] T.C. Lu, L.B. Lin, S.Y. Wu, J. Chen, Y.Y. Zhang, Influence of neutron irradiation and its post-annealing on optical absorption of rutile, Nucl. Instrum. Methods Phys. Res. Sect. B Beam Interact. Mater. Atoms 191 (2002) 236–240.
[78] M. Amer, M.W. Barsoum, T. El-Raghy, I. Weiss, S. Leclair, D. Liptak, The Raman spectrum of Ti_3SiC_2, J. Appl. Phys. 84 (1998) 5817–5819.
[79] B.H. Lohse, A. Calka, D. Wexler, Raman spectroscopy sheds new light on TiC formation during the controlled milling of titanium and carbon, J. Alloys Compd. 434 (2007) 405–409.
[80] H. Foratirada, H.R. Baharvandi, M.G. Maragheh, Behavior of aqueous titanium carbide suspension and evaluation of the gelcasted green body properties, Mater. Res. 20 (2017) 175–182.
[81] A. Paul, D. Dobson, A. James, Infrared spectroscopy of the TiO_2/Aqueous solution interface, Langmuir 15 (1999) 2402–2408.
[82] I. Ali, T. Agayev, G.T. Imanova, H. Mahmudov, S. Musayeva, O.M.L. Alharbi, M. N. Siddiqui, Effective hydrogen generation using water-n-hexane-ZrO_2 system: effect of temperature and radiation irradiation time, Mater. Lett. 340 (2023), 134188.
[83] I. Ali, G.T. Imanova, H.M. Albishri, W.H. Alshitari, M. Locatelli, M.N. Siddiqui, A. M. Hameed, An ionic-liquid-imprinted nanocomposite adsorbent: simulation, kinetics and thermodynamic studies of triclosan endocrine disturbing water contaminant removal, Molecules 27 (2022) 5358.
[84] T.N. Agayev, N.N. Gadzhieva, S.Z. Melikova, Fourier transform IR spectroscopic study of Nano-ZrO_2+Nano-SiO_2+Nano-H_2O systems upon the action of gamma radiation, J. Appl. Spectrosc. 85 (2018) 365–368.
[85] E. Billeter, Z. Łodziana, A. Borgschulte, Surface properties of the hydrogen–titanium system, J. Phys. Chem. C 125 (2021) 25339–25349.
[86] https://materialsproject.org/materials/mp-24726.
[87] S.E. Stein, R.L. Brown, Prediction of carbon-hydrogen bond dissociation energies for polycyclic aromatic hydrocarbons of arbitrary size, J. Am. Chem. 113 (1991) 181–193.
[88] B.E.F. Constance, B.K. Rao, Position of hydrogen atom in a vacancy in aluminum metal - an ab initio study, Rev. Adv. Mater. Sci. 5 (2003) 17–23.
[89] E. Demir, E. Popov, M. Mirzayev, L. Slavov, D. Neov, A. Donkov, K. Siemek, T. Vershinina, I. Genov, A. Beskrovnyi, V. Skuratov, K. Krezhov, P. Horodek, F. Mamedov, A. Valizade, O. Vural, Effects of swift heavy ions at different fluencies on WC-6Co hard metal alloy, Int. J. Refract. Metals Hard Mater. 106 (2022), 105865.
[90] H.C. Wu, A. Kumar, J. Wang, X.F. Bi, C.N. Tomé, Z. Zhang, S.X. Mao, Rolling-induced face centered cubic titanium in hexagonal close packed titanium at room temperature, Sci. Rep. 6 (2016), 24370.
[91] A.A. Donkov, E.P. Popov, Z.A. Sharipov, M.N. Mirzayev, A. Olejniczak, K. Siemek, P. Horodek, Numerical study of graphene protective properties for copper, iron, or tungsten substrates under different types of irradiation (proton, alpha particles, and particle clusters), AIP Conf. Proc. 2551 (2022), 030001.
[92] P. Gopalan, R. Rajaraman, B. Viswanathan, K.P. Gopinathan, The kinetics of formation and growth of TiC precipitates in Ti-modified stainless steel studied by positron annihilation spectroscopy, J. Nucl. Mater. 256 (1998) 229–234.